

# Nonmesonic Hyperon Weak Decay Spectra in ${}_{\Lambda}^{12}\text{C}$

I. Gonzalez<sup>1,2</sup>, A. Deppman<sup>1</sup>, S. Duarte<sup>3</sup>, F. Krmpotić<sup>4</sup>, M. S. Hussein<sup>1</sup>, C. Barbero<sup>4,5</sup>

<sup>1</sup> Instituto de Física, Universidad de São Paulo, São Paulo, Brasil

<sup>2</sup> Instituto de Tecnologías y Ciencias Aplicadas, Havana, Cuba

<sup>3</sup> Centro Brasileiro de Pesquisas Físicas, Rio de Janeiro, Brasil

<sup>4</sup> Instituto de Física La Plata, Universidad Nacional de La Plata, La Plata, Argentina

<sup>5</sup> Departamento de Física, Universidad Nacional de La Plata, La Plata, Argentina

E-mail: israel.gonzalezmedina@gmail.com, adeppman@gmail.com, sbd@cbpf.br, krmpotic@fisica.unlp.edu.ar, hussein@if.usp.br, barbero@fisica.unlp.edu.ar

**Abstract.** We study the nonmesonic weak decay (NMWD)  $\Lambda N \rightarrow nN$  of the  ${}_{\Lambda}^{12}\text{C}$  hypernucleus induced by the nucleon  $N = n, p$  with transition rate  $\Gamma_N$ . The nuclear process is described by the interplay of two models; one describing the NMWD of hyperon  $\Lambda$  in the nuclear environment, and the other taking into account the Final State Interaction (FSI) of the two outgoing nucleons with the residual nucleus. The first one is done in the framework of the Independent-Particle Shell-Model (IPSM), with the decay dynamics represented by the exchange of  $\pi + \eta + K + \rho + \omega + K^*$  mesons with usual parametrization. For the second one is used a time dependent multicollisional intranuclear cascade schema (implemented in the CRISP code - Collaboration Rio-São Paulo). The results obtained for inclusive and exclusive kinetic energy spectra, and the angular correlation are compared with recent data from KEK and FINUDA experiments. The calculated ratio  $(\Gamma_n/\Gamma_p)^{\text{FSI}}$ , between the numbers of emitted back-to-back  $nn$  and  $np$  pairs, is in good agreement with the experimental data.

## 1. Introduction

Since the mesonic channel  $\Lambda \rightarrow \pi N$  is strongly inhibited inside nuclei due to Pauli blocking, the nonmesonic weak decay (NMWD)  $\Lambda N \rightarrow nN$  emerges as the dominant channel. This primary decay can be induced by a neutron ( $\Lambda n \rightarrow nn$ ) or a proton ( $\Lambda p \rightarrow np$ ) with widths  $\Gamma_n$  and  $\Gamma_p$ , respectively. During the last two decades quite significant efforts have been invested in solving the so called 'NMWD puzzle'. This puzzle is related to the large discrepancy between earlier experimental data and theoretical predictions on the NMWD spectra, that yield information about both the primary nonmesonic decay, and the subsequent Final State Interactions (FSI) originated by the nuclear medium. The main aim of the present work is to analyze in which way the FSI modify the spectra obtained within the Independent Particle Shell Model (IPSM), and to find out to what extent it is possible in this way to explain the experimental data. The spectra that we are interested in are: 1) the single-nucleon spectra  $S_N(E_N)$ , as a function of one-nucleon energy  $E_N$ , and 2) the two-particle-coincidence spectra as a function of: i) the sum of kinetic energies  $E_n + E_N \equiv E_{nN}$ ,  $S_N(E_{nN})$ , and ii) the opening angle  $\theta_{nN}$ ,  $S_N(\cos \theta_{nN})$ . The explicit relationships for these transition probability densities can be obtained by performing

derivatives on the appropriate equation for  $\Gamma_N$  [1, 2, 3, 4], *i.e.*,

$$S_N(E_N) = \frac{d\Gamma_N}{dE_N}, \quad S_N(E_{nN}) = \frac{d\Gamma_N}{dE_{nN}}, \quad S_N(\cos \theta_{nN}) = \frac{d\Gamma_N}{d \cos \theta_{nN}}. \quad (1)$$

The measured spectra are obtained by counting the number of emitted nucleons  $\Delta N_N$  within the energy bin  $\Delta E = 10$  MeV, or the angular bin  $\Delta \cos \theta = 0.05$ , always corrected by the detection efficiency. Here we take advantage of the fact that in most of the KEK experiments [5, 6, 7]  $\Delta N_N$  are normalized to the number of NMWD processes,  $N_{NM}$ , while for the FINUDA proton spectra [8, 9] we have at our disposal also the number of produced hypernuclei  $N_H$ . Therefore, we can explore the following relationships

$$\frac{\Delta N_N}{N_{NM}} = \frac{\Delta \Gamma_N}{\Gamma_{NM}}, \quad \frac{\Delta N_N}{N_H} = \frac{\Delta \Gamma_N}{\Gamma_H}, \quad (2)$$

where  $\Delta \Gamma_N$  is the emission rate of protons within the experimentally fixed bin, and  $\Gamma_{NM}$  and  $\Gamma_H$  are, respectively, the NMWD rate and the total hypernuclear decay rate. It could be worth noting that  $\Gamma_H \equiv \Gamma_M + \Gamma_{NM}$ , *i.e.*, is the sum of mesonic and nonmesonic decay rates. It is not clear whether one should use experimental or theoretical values for the rates  $\Gamma_{NM}$ , and  $\Gamma_H$ , and we will adopt the first possibility. Then the correspondences between the theory and data are

$$\Delta \Gamma_N^{th} \iff \Delta \Gamma_N^{exp} = \Gamma_{NM} \left. \frac{\Delta N_N}{N_{NM}} \right|_{KEK} = \Gamma_H \left. \frac{\Delta N_N}{N_H} \right|_{FINUDA}. \quad (3)$$

For  $^{12}\text{C}$   $\Gamma_{NM} = 0.95 \pm 0.04$  [6], and  $\Gamma_H = 1.21 \pm 0.21$  [10]. The theoretical decay widths  $\Delta \Gamma_N^{th}$  are:  $\Delta \Gamma_N(E_N) = S_N(E_N)\Delta E$ ,  $\Delta \Gamma_N(E_{nN}) = S_N(E_{nN})\Delta E$ , and  $\Delta \Gamma_N(\cos \theta_{nN}) = S_N(\cos \theta_{nN})\Delta \cos \theta$  for the spectra explained in 1) and 2). As the one-proton (one-neutron) induced decay prompts the emission of an  $np$  ( $nn$ ) pair the total neutron kinetic energy width is  $\Delta \Gamma_{nt}(E_n) = (S_p(E_n) + 2S_n(E_n))\Delta E$ . For  $\Delta \Gamma_p(E_p)$ ,  $\Delta \Gamma_{nt}(E_n)$ , and  $\Delta \Gamma_N(\cos \theta_{nN})$  are available the data, with the corresponding errors. As for the kinetic energy sums, only the data for yields  $\Delta Y_N(E_{nN})$  were reported so far, without specifying their errors [5]. It is not known how  $\Delta \Gamma_N(E_{nN})$  and  $\Delta Y_N(E_{nN})$  are related with each other, and thus one is forced here to normalize the theoretical results to the data in a similar way as done in Ref. [2], *i.e.*,

$$\Delta Y_N(E_{nN}) = \frac{\bar{Y}_N^{exp}}{\bar{\Gamma}_N} \bar{S}_N(E_{nN})\Delta E, \quad (4)$$

where

$$\bar{Y}_N^{exp} = \sum_{i=1}^m \Delta Y_N^{exp}(E_{nN}^i), \quad \bar{\Gamma}_N = \sum_{i=1}^m S_N(E_{nN}^i)\Delta E, \quad (5)$$

with  $m$  being the number of kinetic energy sum bins, and the barred quantities indicate that and they are constructed with events constrained to  $E_N > 30$  MeV, and  $\cos \theta_{nN} < -0.7$ .

## 2. Independent Particle Shell Model for the primary NMWD

Within the IPSM the spectra defined in (1) read [1, 2, 3, 4]:

$$S_N(E_N) = (A-2) \frac{8M^3}{\pi} \sum_{j_N} \int_{-1}^{+1} d \cos \theta_{nN} \sqrt{\frac{E_N}{E'_N}} E_n \mathcal{F}_{j_N}(pP), \quad (6)$$

$$S_N(\cos \theta_{nN}) = (A-2) \frac{8M^3}{\pi} \sum_{j_N} \int_0^{\tilde{E}_{j_N}} dE_N \sqrt{\frac{E_N}{E'_N}} E_n \mathcal{F}_{j_N}(pP), \quad (7)$$

$$S_N(E_{nN}) = \frac{4M^3}{\pi} \sqrt{A(A-2)^3} \sum_{j_N} \sqrt{(\Delta_{j_N} - E_{nN})(E_{nN} - \tilde{\Delta}_{j_N})} \mathcal{F}_{j_N}(pP), \quad (8)$$

where the summation goes over all occupied single-particle states  $j \equiv \{nlj\}$  for a given  $N = p, n$ , and

$$E'_N = (A-2)(A-1)\Delta_{j_N} - E_N[(A-1)^2 - \cos^2 \theta_{nN}], \quad (9)$$

$$E_n = \left[ \sqrt{E'_N} - \sqrt{E_N} \cos \theta_{nN} \right]^2 (A-1)^{-2}, \quad \tilde{E}_{j_N} = \frac{A-1}{A} \Delta_{j_N}, \quad (10)$$

$$\Delta_{j_N} = \Delta + \varepsilon_\Lambda + \varepsilon_{j_N}, \quad \tilde{\Delta}_{j_N} = \Delta_{j_N} \frac{A-2}{A}. \quad (11)$$

$A$  is the nuclear mass,  $\varepsilon$ 's are the single-particle energies, and  $\Delta = M_\Lambda - M$  is the mass difference between the  $\Lambda$ -hyperon and the nucleon. The quantity  $\mathcal{F}_{j_N}(pP)$  contains the isospin dependence, as well as the dynamics, which is described by exchanges of complete pseudoscalar ( $\pi, K, \eta$ ) and vector ( $\rho, \omega, K^*$ ) meson octets with the weak coupling constants from Refs. [11, 12]. It is defined in Eq. (42) of Ref. [3], and depends on center of mass and relative momenta of the  $nN$  pairs,

$$P = \sqrt{(A-2)(2M\Delta_{j_N} - p_n^2 - p_N^2)}, \quad p = \sqrt{M\Delta_{j_N} - \frac{A}{4(A-2)}P^2}, \quad (12)$$

with  $p_n$ , and  $p_N$  being the momenta of the emitted particles.

### 3. Monte Carlo calculation of FSI with CRISP

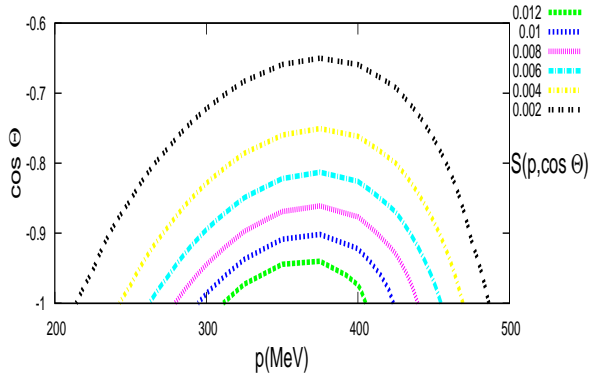


**Figure 1.** Two-dimensional spectrum for protons  $S(p_p, \cos \theta_{np})$  as evaluated from the IPSM Eq. (13).

After having modelled the primary process, we investigate the FSI through the time evolution of Monte Carlo samples constructed to represent the decaying nuclear system, making use of a time dependent multicollisional intranuclear cascade schema (implemented in the CRISP code - Collaboration Rio-São Paulo). The initial sample configurations are spherically shaped portions

of cold Fermi gas with  $A-2$  nucleons, where are incorporated the two energetic intruder nucleons resulting from the primary process, with the IPSM spectra

$$S_N(p_N, \cos \theta_{nN}) = \frac{d^2\Gamma_N}{dp_N d \cos \theta_{nN}} = (A-2) \frac{4M}{\pi} \sum_{j_N} p_N^2 p_n^2 \mathcal{F}_{j_N}(pP), \quad (13)$$

which are shown in Fig. 1 for the emission of the  $np$  pair, and are the starting configuration for the time evolution of the  $A$ -nucleon system, following the sequence of all possible binaries collisions between nucleons. A square well potential is included to mimic the nuclear surface, keeping the low energy nucleons bound within the system. The depth of this potential well is properly chosen in order to have an unperturbed initial configuration without nucleon loss. In fact, the potential confines low energy nucleons through internal reflections, and permits refractions/deflections of energetic nucleons, as dictated by the tunnelling probability of the charged particles through the nuclear Coulomb barrier [13].

The time order of the nucleon-nucleon collisions during the evolution of the system is reconstructed after each collision between pairs of particles, and their displacement inside the nucleus. Consequently, the many-body configurations are followed step by step in phase space, and in time. The cascade phase is ended when no particle is able to leave the nuclear volume, and the number of bound nucleons in the residual nucleus does not change anymore. However, the system still can present some excitation energy compared to a cold nucleon Fermi gas. A thermal decay chain is performed to cool down the post cascade nuclear system by emission of protons, neutrons, and alpha particles, in competition with the fission process [14]. Briefly, the FSI were calculated through a Monte Carlo simulation of all nuclear processes after the primordial NMWD [13, 14, 15, 16, 17], including important features, such as the Pauli blocking within both elastic and inelastic nucleon-nucleon collisions [13, 17].

Note that the interplay between the IPSM and the intranuclear cascade calculation is done through the initial configuration for the Monte Carlo simulation, since the two intruder nucleons in initial sample configurations have their energies, momenta, and opening angle determined stochastically from Eq. (13). Another important bridge between the two models is the choice of the isospins for the two nucleons that start the cascade process. This is also done via a Monte Carlo sampling of the outgoing channel according to the IPSM value for the  $\Gamma_n/\Gamma_p$  ratio in the primary NMWD process.

#### 4. Result and discussion

In Fig. 2 are compared the calculated inclusive proton (left panel), and neutron (right panel) spectra with the KEK [6, 7], and FINUDA [8, 9] data. It is well known that the SFI modify the corresponding IPSM spectra  $\Delta\Gamma_N(E_N) = S_N(E_N)\Delta E$ , with  $S_N(E_N)$  given by (6), by promoting particles from the high energy region towards the low energy region. From the figure one can see that the FSI mechanism is engendered by the interplay between contributions coming from the cascade regime emission, and those induced by the evaporation of the warm residual post-cascade nucleus. The enhancement at low energy induced by the first effect agrees with data, while the quenching at high energy produced by the second effect is too strong, in disagreement with the data. We also note that the threshold for the opening of the cascade effect is sharper in the  $pn$  than in the  $nn$  case due to the Coulomb barrier.

In left and right panels of Fig. 3 we show the angular distributions for the  $nn$  and  $np$  channels, respectively. We get reasonable agreement with experimental results in the case of the  $nn$  channel, but our calculation does not reproduce the peak observed experimentally in the back-to-back region for the  $np$  channel. This is due to too strong FSI quenching on the IPSM spectra  $S_p(\cos \theta_{np})$  given by (7).

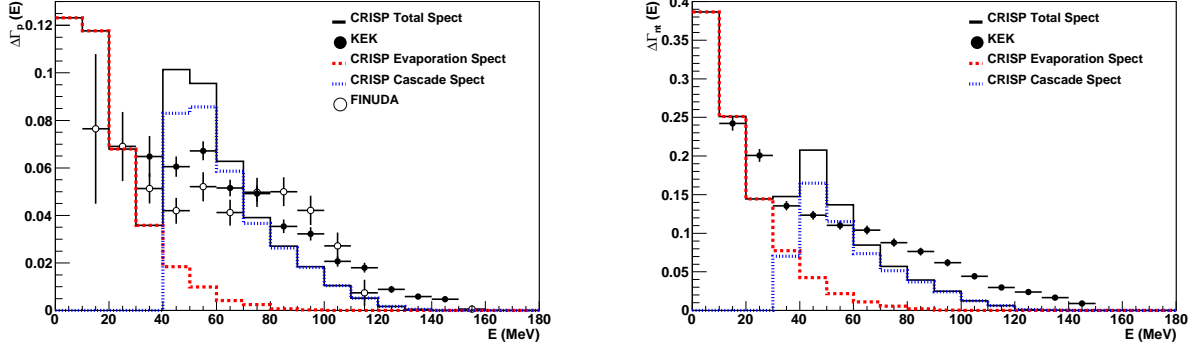


**Figure 2.** Calculated inclusive single particle spectra (full histogram), compared to the data from Ref. [6, 7] in open circles, and from Ref. [8, 9] in full circles. The dotted histogram are the contribution coming from cascade regime of the process and the dashed one depicts the contribution of particles evaporation of the warm post-cascade residual nucleus.

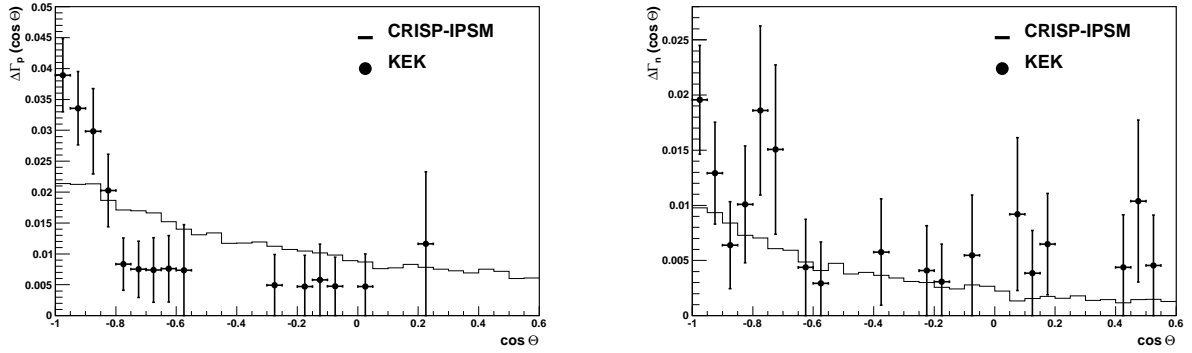


**Figure 3.** Angular distribution of the  $np$ -pairs (left panel), and the  $nn$ -pair (right panel) compared to experimental data from Ref. [6, 7].

In the right panel of Fig. 4 we show the total kinetic energy of the correlated  $np$  pairs, and compared them to the KEK experimental data [5]. The theoretical predictions are normalized to the data according to Eqs. (4), and (5). We observed that both the centroid and width of the theoretical spectrum are quite similar to the experimental one, covering a broad energy interval from  $\simeq 80$  MeV up to the  $Q$ -value at  $\simeq 150$  MeV. For the  $nn$  channel, as shown in the left panel of Fig. 4, the agreement between calculated and data is not so good as in the  $np$  case. However, we would like to draw attention to the fact that, because of very low statistic, which in turn is due to difficulties in detecting two neutrons in coincidence, the experimental histogram contains relatively small number of events.

We have also calculated the ratio between  $\Gamma_n$  and  $\Gamma_p$  by considering the emitted  $nn$  and  $np$  pairs in the back-to-back opening angle region  $\cos \theta_{nN} \leq -0.7$ , getting the value  $(\Gamma_n/\Gamma_p)^{\text{FSI}} = 0.454$ , in nice agreement with the recently reported experimental result  $(\Gamma_n/\Gamma_p)^{\text{exp}} = 0.53 \pm 0.13$  [5], where the background uncertainty is 0.05. At this point it is interesting to mention that the IPISM model calculation yields the value  $(\Gamma_n/\Gamma_p)^{\text{IPISM}} = 0.262$ . We can attribute the

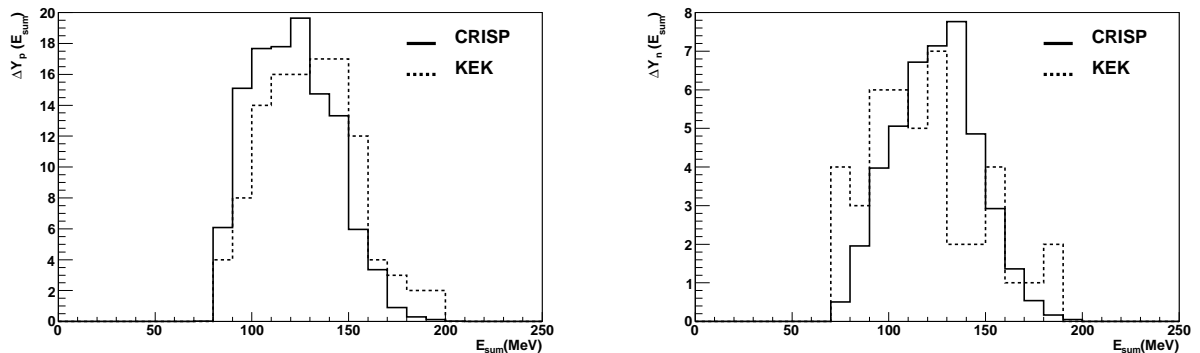


**Figure 4.** The kinetic energy distribution of the  $nN$  pairs calculated for events with strong back-to-back correlation of the opening angles. The full histograms are the results from the calculation, and dotted histograms are data from Ref. [5]. To define the back-to-back events we have adopted the same low energy cutoff, and the same angle interval as done in the experiment.

difference between  $(\Gamma_n/\Gamma_p)^{\text{IPSM}}$ , and  $(\Gamma_n/\Gamma_p)^{\text{FSI}}$  to a possible depletion in the proton emission due the Coulomb barrier at the residual nucleus surface, implying that a neutron produced during the primary process have higher probability of leaving the nucleus than a primary proton.

## 5. Conclusions

The role played by the FSI on the NMWD has been investigated. For the inclusive nucleon spectra we have depicted separately the contributions coming from the cascade phase, and the low energy ones coming from the particle evaporation process in the post cascade phase regime. The importance of the latter nucleons in reproducing the experimental data was put in evidence. In the analysis of angular distributions, we have obtained a reasonable agreement for the  $nn$  channel, while the results for the  $np$  channel still need to be improved. From the comparison of the  $\Gamma_n/\Gamma_p$  ratios before and after the inclusion of FSI, one sees that these interactions increase the  $n/p$  ratio by a factor of  $\sim 1.8$ , yielding in this way the agreement with the measurement.

## References

- [1] Barbero C, Galeão A P, Hussein M S and Krmpotić F 2008 *Phys. Rev. C* **78** 044312
- [2] Bauer E, Galeão A P, Hussein M S, Krmpotić F and Parker J D 2009 *Phys. Lett. B* **674** 109
- [3] Krmpotić F, Galeão A P, Hussein M S 2010 *AIP Conf. Proc.* **1245** 51
- [4] Krmpotić F 2010 *Phys. Rev. C* **82** 055204
- [5] Kim M J *et al* 2006 *Phys. Lett. B* **641** 28
- [6] Kim M J *et al* 2009 *Phys. Rev. Lett.* **103** 182502
- [7] Bhang H. 2010, private communication
- [8] Agnello M *et al* 2010 *Phys. Lett. B* **685** 247
- [9] Garbarino G. 2010, private communication
- [10] M. Agnello, *et al.*, *Phys. Lett. B* **681** (2009) 139.
- [11] A. Parreño, A. Ramos, and C. Bennhold 1997 *Phys. Rev. C* **56** 339-364
- [12] Parreño A and Ramos A 2001 *Phys. Rev. C* **65** 015204
- [13] Deppman A *et al.* 2002 *Comp. Phys. Comm.* **145** 385
- [14] Deppman A, Duarte S B, Silva G, Tavares O A P, Anéfalos S, Arruda-Neto J D T and Rodrigues T E 2004 *J. Phys. G* **30** 12
- [15] Gonçalves M, de Pina S, Lima D A, Milomen W, Medeiros E L and Duarte S B 1997 *Phys. Lett. B* **406** 1
- [16] de Pina S, De Oliveira E C, Medeiros E L, Duarte S B and Gonçalves M 1998 *Phys. Lett. B* **434** 1
- [17] Deppman A, Tavares O A P, Duarte S B, de Oliveira E C, Arruda-Neto J D T, de Pina S R, Likhachev V P, Rodriguez O, Mesa J and Gonçalves M 2001 *Phys. Rev. Lett.* **87** 182701